Article

Not peer-reviewed version

# Analyzing Power Law Extensions of Newtonian Gravity Using Differential Force Measurements

Thomas Bsaibes and Ricardo Decca *

Posted Date: 26 February 2024

doi: 10.20944/preprints202402.1416.v1

Keywords: hypothetical interactions; power-type potentials; constraints on hypothetical particles

 doi:10.20944/preprints202402.1416.v1



*Article*

# Analyzing Power Law Extensions of Newtonian Gravity Using Differential Force Measurements

**Thomas Bsaibes and Ricardo Decca ***

Indiana University Indianapolis

* Correspondence: rdecca@iupui.edu

**Abstract:** The Standard Model is not a complete description of reality; it omits the existence of dark matter, dark energy, and an explanation as to why no CP violation has been observed. However, some of these phenomena could be explained through a new force mediated by a new boson. If such a boson were massless it would result in a power law potential and if massive the interaction would be Yukawa-like. A previous experiment employing a micro-mechanical oscillator and a spherical test mass interactions was successful in placing the best limits on a mass-mass Yukawa-like interaction, but the data was never analyzed in the context of a power law. Here that data is analyzed considering a power law for powers $n$ = 1-5 where $n$ is the number of boson exchanges. The results show that the limits obtained through power law analysis of this data are not better than the currently accepted limits. A discussion of an experiment design capable of producing better limits on power law extensions to the Standard Model is presented, and suggests micro mechanical oscillators based experiment remains capable of improving the limits by at least one order of magnitude.

**Keywords:** hypothetical interactions; power-type potentials; constraints on hypothetical particles

## 1. Introduction

The success of the Standard Model (SM) in describing matter and interactions cannot be over stated, but it is not a complete description: it does not explain dark matter and dark energy [1], it predicts CP violations in the strong force which have not yet been observed [1–3], and there is no quantized description of gravity [1]. This incompleteness has lead to many theories to fill the gaps of the SM.

One such approach is hypothesizing an interaction mediated by an as of yet undiscovered boson [4,5]. If the hypothetical boson is massive it leads to Yukawa-like interactions [6], but if it is massless the interaction will be parameterized with a power law [7]. This power law is typically written as a correction to Newtonian gravity, and for two point masses is expressed as

$$U = \frac{-Gm_1m_2}{r}\left(1+\Lambda_n\left(\frac{r_0}{r}\right)^{n-1}\right) \tag{1}$$

where $G$ is Newton's gravitational constant, $m_1$ and $m_2$ are point masses separated by a distance $r$, $\Lambda_n$ is the strength of the correction relative to gravity for a particular power of $n$, and $r_0$ is a constant used to preserve the dimension of the interaction; in this work $r_0 = 1 \times 10^{-15}$ m [8].

Previous experiments to probe both power law and Yukawa-like deviations in Newtonian gravity [8–10]. One experiment to probe hypothetical Yukawa-like interactions was carried out in 2016 [11]. The Yukawa-like interaction is of the form

$$U = \frac{-Gm_1m_2}{r}\left(1+\alpha e^{r/\lambda}\right) \tag{2}$$

was probed and placed the best limits on $\alpha$ for a range of $\lambda \in (30, 8000)$ nm, where $\alpha$ is the strength of the correction and $\lambda$ is the Compton wavelength of a massive hypothetical boson [11]. The experiment consisted of a spherical test mass attached to micro-mechanical oscillator, which was brought within 200 nm of a source mass of Au-Si sector and the force was measured between the two masses. The set

 doi:10.20944/preprints202402.1416.v1



up was not designed to probe power law extensions of the SM and was expected to not be sensitive enough to improve those limits. However, a reanalysis of the force measurements from [11] and a full analysis with the data was never carried out in the context of a power law.

Power law models are not explicitly mentioned in the pursuit of experimental evidence of dark matter [12–19]. This work does a full analysis considering power law extensions of the SM on the force measurements in [11] as well as on new data. The limits obtained are not an improvement over the current best limits [8,10], so we discuss what would need to be done for the approach in [11] to improve limits on power law extensions to the SM.

## 2. Materials and Methods

The study published in 2016 [11] used a differential force measurement technique between a spherical test mass attached to a micro-mechanical oscillator and a source mass. The test mass was a sphere composed of 3 layers; a central sapphire core with a $149.3 \pm 0.2$ $\mu$m radius covered by 10 nm of Cr followed by 250 nm of Au (see Figure 1 for a cross sectional diagram of the test and source mass). The sphere was glued to a $500 \times 500$ $\mu$m micro-mechanical oscillator and the system had a quality factor $Q \sim 7200$. The deflection of the test mass was measured through a change in capacitance between the oscillator's plate and electrodes located below the plate.

The source mass was a layered structure of BK7 Schott glass followed by a $2.10 \pm 0.02$ $\mu$m layer of alternating sectors of Au and Si. Both Au and Si sectors shared a common layer of a $10 \pm 1$ nm Cr wetting layer on top of which was a 150 nm Au layer covering the sample. The shared top Au layer thickness was chosen to be larger than the effective penetration depth of the Casimir force. In this way the contribution due to the Casimir force is the same whether the test mass is located over a Si sector or a Au sector and leads to a Casimir-less measuring technique as described in [20]. The test mass was brought to within 200 nm of the source mass's surface and at this separation the minimum detectable force is 12 fN/$\sqrt{\text{Hz}}$. The source mass was rotated so that the sectors alternated under the test mass at the oscillator's resonant frequency. Doing so makes the experiment select the first harmonic of the force commensurate with the period of the samples.

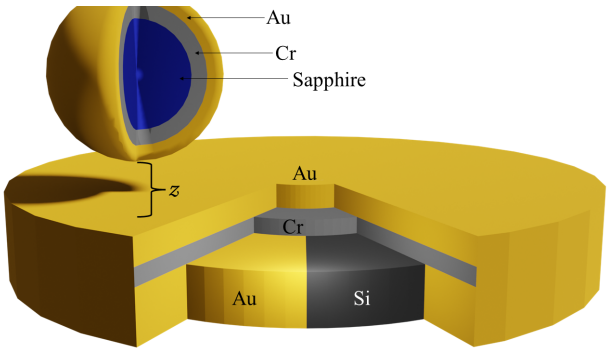


**Figure 1.** Cut out view (not to scale) of the source mass and test mass showing the individual layers. The source mass has top Au layer, followed by a Cr layer, and then the alternating Si and Au regions. The test mass has a central sapphire core (shown in blue) coated with Cr and Au. The $z$ indicates the separation and the direction which the experiment is sensitive.

While the source masses used to set limits on the Yukawa-like interaction [11] had upwards of 300 Au-Si sectors, there were source masses that had two, 1 mm wide, sectors of alternating gold and silicon, as depicted in Figure 2. One sample had an inner radius of 2.5 mm and the other had an inner radius of 5 mm. The layered structure is the same as the 300 sector samples except the wetting layer is Ti. The data taken with these larger source masses were previously not analyzed.

 doi:10.20944/preprints202402.1416.v1



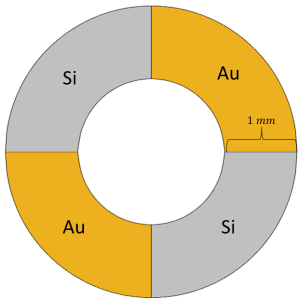


**Figure 2.** A diagram showing the new source mass geometry, regions alternate between gold and silicon.

To extract limits on $\Lambda_n$, the force due to the potential expressed in Eq. 1 was calculated by integrating over the experimental geometry. First, the interaction between a spherical test mass and an arbitrary point in the source mass was calculated analytically with a coordinate system centered at the sphere, shown as the unprimed coordinate system in Figure 3, using spherical coordinates $(\tilde{r}, \theta, \phi)$ where $\theta$ and $\phi$ are the polar and azimuthal angle respectively. The potential energy between the sphere and the source mass is

$$U = -2\pi G\rho_1\rho_2\Lambda_n r_0^{n-1} \iiint \left( \frac{1}{\psi(2-n)} \left[ \frac{R(\psi-R)^{3-n}}{3-n} + \frac{(\psi-R)^{4-n}}{(4-n)(3-n)} + \frac{R(\psi+R)^{3-n}}{3-n} - \frac{(\psi+R)^{4-n}}{(4-n)(3-n)} \right] \right) dV_{sm} \tag{3}$$

where $R$ is the radius of the sphere, $\rho_1$ and $\rho_2$ are the densities of the sphere and the point respectively, $\psi$ is the distance from the center of the sphere to the arbitrary point in the source mass and $dV_{sm}$ is the differential volume of the source mass, see Appendix A for details. It was verified that Eq. 3 does not diverge for $n = 2, 3$, and 4 by taking the limit of Eq. 3 as $n \to 2, 3$, and 4 respectively, these limits can be seen in Appendix A. The integrals over the source mass were carried out using cylindrical coordinates $(\varrho, \theta', z')$ in the primed coordinate system, see Figure 3, centered in the middle of the source mass. In the primed coordinate system

$$\psi = \sqrt{\varrho^2 - 2\varrho\varrho_s\cos(\theta' - \theta_s) + \varrho_s^2 + (z' - z_s)^2} \tag{4}$$

where $\varrho$ is the radial variable integrated between the inner and outer radius of the sample, $\theta'$ is the angular extent of the sample, $\varrho_s$ is the radial distance to the sphere, $\theta_s$ is the angular postion of the sphere, $z_s$ is the vertical position of the center of the sphere, and $z'$ is the vertical coordinate integrated over the thickness of the sample.

The experiment is only sensitive to forces in the vertical direction, normally calculating the force in the $z$ direction would be done by

$$F_z = -\frac{\partial}{\partial z'} U \tag{5}$$

where $dF_z$ is the differential force in the vertical direction that needs to be integrated over the geometry of the source mass. However, since Eq. 5 needs to be integrated along $z'$ doing the derivative explicitly can be avoided because the operations are the inverse of each other; meaning the integral of Eq. 5 over the source mass in $z$ is simply the difference of Eq. 3 evaluated at the $z'$ integration limits of the source mass, $z_1$ and $z_2$.

$$F_z^{(n)} = \iint (U^{(n)}(z_1) - U^{(n)}(z_2)) dA_{sm} \tag{6}$$

where $dA_{sm}$ is the area element of the source mass which remains to be integrated. A polar coordinate system centered at the center of the sample, the primed coordinate system in Figure 3, is used for

 doi:10.20944/preprints202402.1416.v1



the last two integrals. The area element is expressed as $dA_{sm} = \varrho d\varrho d\theta'$ where $(\varrho, \theta')$ are the polar coordinates in the primed system. The integrals over $\varrho$ and $\theta'$ were done numerically with Python code using SciPy packages [21].

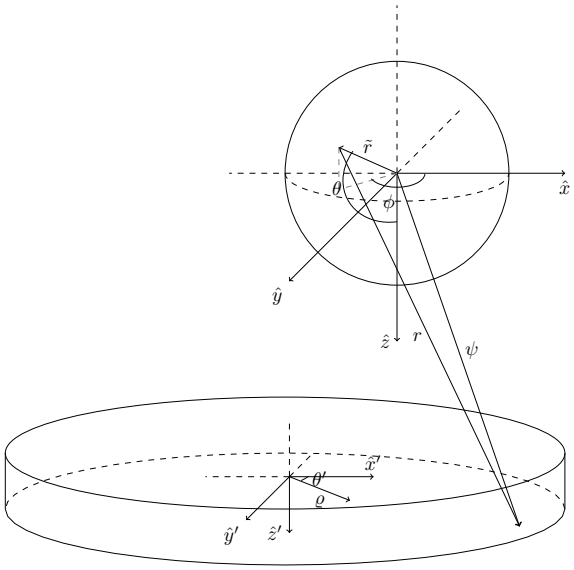


**Figure 3.** The coordinate system and geometry over which the test mass and source mass were integrated. The unprimed coordinate system is used to integrate over the sphere. $\theta$ and $\phi$ are the polar and azimuthal angle respectively, $\psi$ is the distance from the center of the sphere to an arbitrary point in the source mass, and $r$ is the separation between points in the sphere and points in the disk. The primed coordinate system is the system used to integrate the geometry of the source mass. $\theta'$ is the polar angle in the primed coordinates and $\varrho$ is the radial variable in the source mass system.

In order to get the correct interaction from the layered geometry, the numerical integrations were carried out three times, once for each of the the three different layers of the test mass. Each test mass layer was considered to be a solid sphere with corresponding radii of $R_{sap} = 149.30$ $\mu$m, $R_{Cr} = 149.31$ $\mu$m, and $R_{Au} = 149.56$ $\mu$m for sapphire, Cr, and Au respectively. As an example for n = 3 the integrations for each layer are

$$F_{Au}^{(3)} = 2\pi G r_0^2 \iint \left( \frac{R_{Au}(\psi(z_2) - \psi(z_1))}{\psi(z_1)\psi(z_2)} + \ln\left( \frac{(\psi(z_1) - R_{Au})(\psi(z_2) + R_{Au})}{(\psi(z_1) + R_{Au})(\psi(z_2) - R_{Au})} \right) \right) dA_{sm} \tag{7}$$

$$F_{Cr}^{(3)} = -2\pi G r_0^2 \iint \left( \frac{R_{Cr}(\psi(z_2) - \psi(z_1))}{\psi(z_1)\psi(z_2)} + \ln\left( \frac{(\psi(z_1) - R_{Cr})(\psi(z_2) + R_{Cr})}{(\psi(z_1) + R_{Cr})(\psi(z_2) - R_{Cr})} \right) \right) dA_{sm} \tag{8}$$

$$F_{Sap}^{(3)} = -2\pi G r_0^2 \iint \left( \frac{R_{Sap}(\psi(z_2) - \psi(z_1))}{\psi(z_1)\psi(z_2)} + \ln\left( \frac{(\psi(z_1) - R_{Sap})(\psi(z_2) + R_{Sap})}{(\psi(z_1) + R_{Sap})(\psi(z_2) - R_{Sap})} \right) \right) dA_{sm} \tag{9}$$

Equations 7,8 and 9 are the integrals over the source mass geometry carried out after the limit of Eq. 3 was taken as $n \to 3$, where $\psi(z_1)$ and $\psi(z_2)$ are Eq. 4 evaluated at $z_1$ and $z_2$ respectively. The integrals for the other powers were done in the same manner. Once the integrals for each test mass layer is carried out, the total force due to the layered structure of the source mass and test mass (Figure 1) is

 doi:10.20944/preprints202402.1416.v1



$$F_z^{(3)} = \Lambda_3(\rho_{Au}-\rho_{Si})((\rho_{Sap}-\rho_{Cr})F_{Sap}^{(3)} + (\rho_{Cr}-\rho_{Au})F_{Cr}^{(3)} + \rho_{Au}F_{Au}^{(3)}) \tag{10}$$

where $\rho_{Au}$, $\rho_{Cr}$, $\rho_{sap}$, and $\rho_{Si}$ are the densities of Au, Cr, sapphire, and Si respectively, $F_z^{(3)}$ indicates the total force in the $z$-direction for the power $n = 3$, and the factor out front, $(\rho_{Au} - \rho_{Si})$, accounts for the difference when the sphere is over a Au or Si in the source mass. Further more, since the first two layers are a shared layer of Au and Cr, the contributions of these layers to the interaction gets subtracted out.

The total force was calculated with the test mass at different angular positions ($\theta_s'$), Figure 4. The amplitude of the first harmonic for a particular power, $A_1^{(n)}$, of the force commensurate with the period, $\Theta$, of the sectors was equated to the error bars of the force measurements.

$$A_1^{(n)} = \frac{2}{\Theta}\int_0^{\Theta} F_z^{(n)} \cos\left(\frac{2\pi\theta_s}{\Theta}\right) d\theta_s \tag{11}$$

The error bar value is $f_{err} = 0.13$ fN at a separation of 300 nm, as shown in Figure 5. Equating the calculated first harmonic of the force to the experimental error bar allows limits on $\Lambda_n$ to be extracted.

$$\Lambda_n = \frac{f_{err}}{A_1^{(n)}} \tag{12}$$

The same method to determine limits was used for the powers of $n = 1$ to 5. Table 1 shows the limits placed on $\Lambda_n$ from both the 300 sector source masses used in [11] and the 4 sector source mass with inner radius of 2.5 mm as depicted in Figure 2.

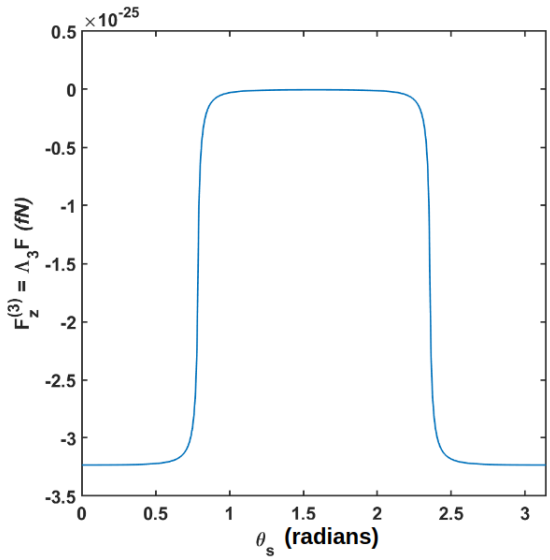


**Figure 4.** The total force as the angular location of the sphere changes, which is equivalent to fixing the location of the sphere and rotating the sample. The first harmonic of the force in accordance with the period of the sectors is calculated and equated to the error bars of the force measurement to extract $\Lambda_n$. This example is from Eq. 10, where $F = \frac{F_z^3}{\Lambda_3}$, $F_z^3$ from Eq. 10.

 doi:10.20944/preprints202402.1416.v1



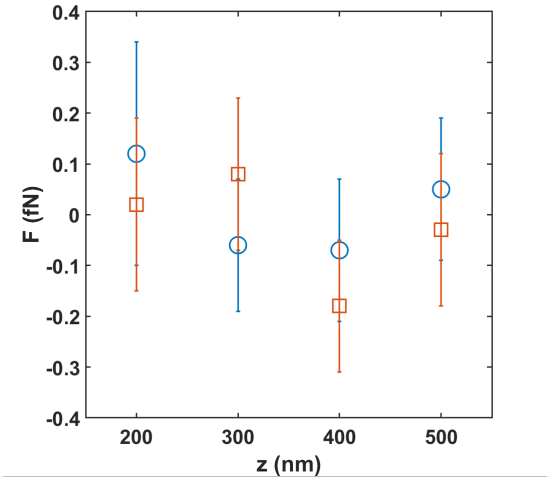


**Figure 5.** Measured force as a function of separation of the large source mass. The blue circle data corresponds to the sample with an inner radius of 2.5 mm and the orange squares are the data from the 5 mm inner radius sample.

**Table 1.** The constraints placed on $\Lambda_n$ from our experiment compared to the limits reported in [8]. The two right most columns are the limits calculated using the data from the many sector samples and the large sector samples.

| n | $\Lambda_n$ from [8] | $\Lambda_n$ Many Sector Sample | $\Lambda_n$ Large Sector Sample |
|---|---|---|---|
| 1 | $1 \times 10^{-9}$ | $8.0 \times 10^{8}$ | $3.0 \times 10^{2}$ |
| 2 | $3.7 \times 10^{8}$ | $6.1 \times 10^{15}$ | $2.5 \times 10^{13}$ |
| 3 | $7.5 \times 10^{19}$ | $7.9 \times 10^{24}$ | $8.8 \times 10^{23}$ |
| 4 | $2.2 \times 10^{31}$ | $1.2 \times 10^{34}$ | $5.2 \times 10^{33}$ |
| 5 | $6.7 \times 10^{42}$ | $1.4 \times 10^{43}$ | $1.0 \times 10^{43}$ |

## 3. Results

The limits presented in Table 1 were calculated using results from an experiment that was not designed to probe power law extensions to the SM. If the source masses were designed with a power law in mind, however, the limits could be further improved. Figure 6 shows the potential limits for $\Lambda_5$ as a function of the sample's radial extent ($\varrho$) for a thickness of 2 mm. The limits have a similar functional dependence with the other dimensions of the sample as the radius increases. The improvement is attributed to the larger volume of interaction improving the sensitivity of the measurement yielding better limits. However, the improvement gained in the limits by increasing the source mass's volume quickly diminishes.

Changing the test mass to also have a larger volume of interaction could provide a small improvement on power law limits. Considering a system, like the one proposed in [22], where the test mass is cylindrical and carrying out a similar analysis as described above with a new test mass, the expected limits using a cylindrical test mass can be calculated. The details of the calculation can be found in Appendix B. The following is the expression of the force between a cylindrical test mass and an infinite slab with thickness $t = 2$ mm along the vertical direction

$$F_5 = \frac{-\pi^2 G \rho_1 \rho_2 L \Lambda_5 r_0^4}{3} \left( \frac{A_2^2}{(R^2 - A_2^2)\sqrt{A_2^2 - R^2}} - \frac{A_1^2}{(R^2 - A_1^2)\sqrt{A_1^2 - R^2}} \right) \tag{13}$$

 doi:10.20944/preprints202402.1416.v1



where $A_1 = d + R_{Au}$, $A_2 = A_1 + t$, and $L = 500$ $\mu$m the length of the cylinder. The expected limits for the powers $n = 1 - 5$ using a cylindrical test mass are listed in Table 2 calculate with the separation $d = 200$ nm. Only the power $n = 5$ is expected to improve by about an order of magnitude using a cylinder.

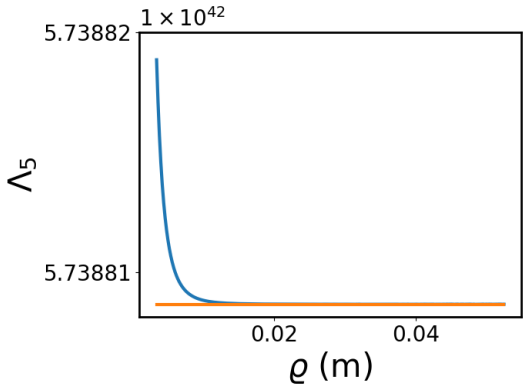


**Figure 6.** The limits on $\Lambda_5$ can be marginally improved if the size of the source mass is designed with power law interactions in mind. Shown here are the estimated limits for n = 5 as a function of the width of the source mass. However the improvement gained by increasing the source mass size quickly diminishes. The constant orange line is the limit that would be achieved as the width of the source mass goes to infinity.

**Table 2.** The constraints that could be placed on $\Lambda_n$ if a cylindrical test mass were used with a source mass designed to probe power law potentials.

| n | $\Lambda_n$ from [8] | Cylindrical Test Mass |
|---|---|---|
| 1 | $1 \times 10^{-9}$ | $6.1 \times 10^{-2}$ |
| 2 | $3.7 \times 10^{8}$ | $4.4 \times 10^{10}$ |
| 3 | $7.5 \times 10^{19}$ | $2.0 \times 10^{22}$ |
| 4 | $2.2 \times 10^{31}$ | $1.1 \times 10^{32}$ |
| 5 | $6.7 \times 10^{42}$ | $2.8 \times 10^{41}$ |

## 4. Conclusions

While these types of mechanical measurements have a high precision even at separations ∼200 nm, this work shows that the size of the masses limit the sensitivity when probing power law interactions. The limit on $\Lambda_5$, reported here to be $1.0 \times 10^{43}$, is expected to improved about an order of magnitude over the best current limits [8] by designing the experiment for power law extensions to Newtonian gravity. Improving the limits of power law extensions to gravity is a challenging endeavor and new methods are needed to continue to make improvements on short range interaction experiments. Several experimental approaches are being developed to test gravity at short distances, seeking signs of deviations potentially due to dark matter effects [12–19]. The description of these new approaches does not explicitly state probing power law extensions to the SM. Researcher should evaluate whether these new techniques are equally suited to test power law models as well as Yukawa-like interactions, which could result in a larger selection of theories being ruled out.

## Appendix A. Detailed Calculation Method for Sphere Test Mass Geometry

$$dU = -G\rho_{tm}\rho_{sm}\Lambda_n r_0^{n-1}\left(\frac{dV_{tm}dV_{sm}}{r^n}\right) \tag{A1}$$

 doi:10.20944/preprints202402.1416.v1



Equation A1 is the differential potential that needs to be integrated to calculate the interaction between the test mass and the source mass, where $G$ is Newton's gravitaional constant, $\rho_{tm}$ ($\rho_{sm}$) is the density of the test mass (source mass), $\Lambda_n$ is the strength of the correction for a particular power $n$, $r_0$ is a constant used to preserve the dimension, $dV_{tm}$ ($dV_{sm}$) is the test mass (source mass) volume element, and $r$ is the distance between a point in the test mass and a point in the source mass and is expressed as

$$r = \sqrt{\tilde{r}^2 + \psi^2 - 2\tilde{r}\psi\cos(\theta)}. \tag{A2}$$

Where $\tilde{r}$ is the radial coordinate of a point in the sphere and has integration limits from zero to the radius of the sphere, $\theta$ is the polar coordinate of the sphere, and $\psi$ is the distance from the center of the spherical test mass to an arbitrary point in the source mass. We use spherical coordinates to integrate the test mass so the test mass volume element is expressed as

$$dV_{tm} = \tilde{r}^2 d\tilde{r} d(\cos(\theta)) d\phi. \tag{A3}$$

The integral over the test mass is carried out as follows

$$dU = -G\rho_{tm}\rho_{sm}\Lambda_n r_0^{n-1}\left(\int_0^R\int_{-1}^1\int_0^{2\pi}\frac{\tilde{r}^2 d\tilde{r} d(\cos(\theta)) d\phi}{(\tilde{r}^2+\psi^2-2\tilde{r}\psi\cos(\theta))^{n/2}}\right) dV_{sm}. \tag{A4}$$

Nothing in Eq. A4 depends on azimuthal angle, $\phi$, so the integral over $\phi$ results in a factor of $2\pi$.

$$dU = -2\pi G\rho_{tm}\rho_{sm}\Lambda_n r_0^{n-1}\left(\int_0^R\int_{-1}^1\frac{\tilde{r}^2 d\tilde{r} d(\cos(\theta))}{(\tilde{r}^2+\psi^2-2\tilde{r}\psi\cos(\theta))^{n/2}}\right) dV_{sm} \tag{A5}$$

Using the following change of variables: $x = \cos(\theta)$ and $u^2 = \tilde{r}^2 - 2\tilde{r}\psi x + \psi^2$, Eq. A5 is now

$$dU = -2\pi G\rho_{tm}\rho_{sm}\Lambda_n r_0^{n-1}\left(\int_0^R\int_{(\psi+\tilde{r})}^{(\psi-\tilde{r})}\frac{\tilde{r}u^{1-n} du d\tilde{r}}{\psi}\right) dV_{sm} \tag{A6}$$

and carrying out the last two integrals for the test mass, we are left with potential between the sphere and an arbitrary point in the source mass.

$$\begin{aligned} dU = \frac{-2\pi G\rho_{tm}\rho_{sm}\Lambda_n r_0^{n-1}}{\psi(2-n)(3-n)(4-n)}\Big(&R(4-n)(\psi-R)^{3-n} + (\psi-R)^{4-n} + R(4-n)(\psi+R)^{3-n} \\ &- (\psi+R)^{4-n}\Big) dV_{sm} \end{aligned} \tag{A7}$$

For n = 2, 3, and 4 Eq. A7 yields $0/0$; as such it needs to be verified that it does not diverge by taking the limits as $n \to 2$, 3, and 4. Taking the limit of Eq. A7

$$\lim_{n\to 2,3,\text{or } 4}\frac{\left(R(4-n)(\psi-R)^{3-n} + (\psi-R)^{4-n} + R(4-n)(\psi+R)^{3-n} - (\psi+R)^{4-n}\right)}{(2-n)(3-n)(4-n)} \tag{A8}$$

and using l'Hôptial's rule to evaluate A8 results in

$$\begin{aligned} \lim_{n\to 2,3,\text{or } 4}\Bigg[&\frac{\left(R((\psi-R)^{3-n}(n-4)\ln(\psi-R) - (\psi-R)^{3-n}) - (\psi-R)^{4-n}\ln(\psi-R)\right)}{-((3-n)(4-n)+(2-n)(4-n)+(2-n)(3-n))} \\ &+\frac{R((\psi+R)^{3-n}(n-4)\ln(\psi+R) - (\psi+R)^{3-n}) + (\psi+R)^{4-n}\ln(\psi+R))}{-((3-n)(4-n)+(2-n)(4-n)+(2-n)(3-n))}\Bigg]. \end{aligned} \tag{A9}$$

Evaluating equation A9 for n = 2, 3, or 4 shows that A7 does not diverge, see Table A1.

 doi:10.20944/preprints202402.1416.v1



**Table A1.** The results of taking the limit of Eq. A9 for powers n = 2, 3, and 4 showing that Eq. A7 does not diverge for those powers.

| n | Limit Result |
|---|---|
| 2 | $R\psi + \frac{(\psi^2-R^2)}{2}\ln\left(\frac{\psi-R}{\psi+R}\right)$ |
| 3 | $-2R - \psi\ln\left(\frac{\psi-R}{\psi+R}\right)$ |
| 4 | $\frac{\psi R}{\psi^2-R^2} - \frac{1}{2}\ln\left(\frac{\psi-R}{\psi+R}\right)$ |

It was verified that integrating A6 the powers n = 2, 3, and 4 yield the same expressions as taking the limit expressed in Eq. A9. Now that it is shown that Eq. A7 does not diverge what is left is to integrate over the source mass.

## Appendix B. Detailed Calculation Method for Cylinder Test Mass Geometry

The starting point to calculate the interaction between an infinite slab and a cylinder is potential

$$dU = -G\rho_{sm}\Lambda_n r_0^{n-1}\left(\frac{dV_{sm}}{r^n}\right). \tag{A10}$$

The procedure to integrate the cylinder-slab geometry is the following

1. integrate over the source mass
2. calculate the field due to the source mass, $\vec{g}$, along the $\hat{z}$
3. calculate the force, $F_z^{(n)} = \vec{g}m_{tm}$, where $m_{tm}$ is the mass of the test mass calculated $m_{tm} = \iiint \rho_{tm}dV_{tm}$

$\rho_{tm}$ is the density of the test mass and $dV_{tm} = dxdydz$ is the volume element of the test mass. The coordinate system used for integrating the infinite slab-cylinder geometry is shown in Figure A1.

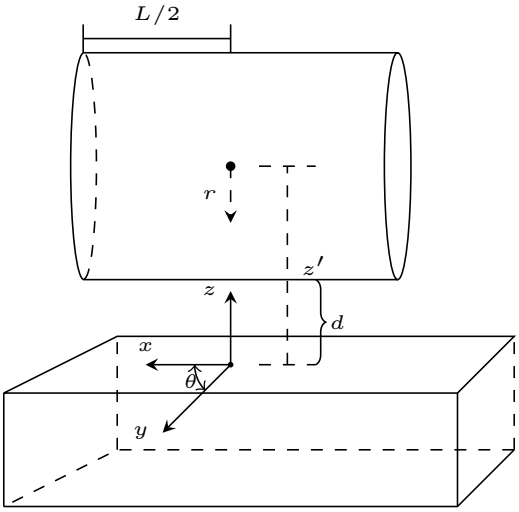


**Figure A1.** The coordinate system used to integrate over the infinite slab-cylinder geometry. $L$ is the length of the cylinder and $d$ is the distance from the top of the slab to the bottom of the cylinder.

First, we will start with the integral over the source mass.

$$dU = -G\rho_{sm}\Lambda_n r_0^{n-1}\iiint \frac{dV_{sm}}{r^n} \tag{A11}$$

$$= -G\rho_{sm}\Lambda_n r_0^{n-1}\iiint \frac{\rho d\rho d\theta dz}{(\rho^2+(z'-z)^2)^{n/2}} \tag{A12}$$

 doi:10.20944/preprints202402.1416.v1



The limits of integration over the source mass are $\rho \in [0,\infty)$,$\theta \in [0,2\pi]$, $z \in [0,-t]$. Integrating over $\theta$ and doing the change of variable $s^2 = \rho^2 + (z'-z)^2$

$$U = -2\pi G\rho_{sm}\Lambda_n r_0^{n-1}\int_{z'-z}^{\infty}\frac{ds}{s^{n-1}} \tag{A13}$$

$$= -2\pi G\rho_{sm}\Lambda_n r_0^{n-1}\int_0^{-t}\frac{dz}{(2-n)(z'-z)^{n-2}} \tag{A14}$$

$$= \frac{-2\pi G\rho_{sm}\Lambda_n r_0^{n-1}}{(2-n)(3-n)}\left(z'^{3-n} - (z'+t)^{3-n}\right) \tag{A15}$$

Equation A15 is used for $n = 1, 4,$ and 5, for $n = 2$ and 3 Eq. A10 was integrated specifically for those powers.

The field is along $\hat{z}$ due to the source mass is calculated by

$$\vec{g} = -\frac{dU}{dz'}\hat{z} \tag{A16}$$

*Appendix B.1.* $n = 1$

$$U = \frac{-2\pi G\rho_{sm}\Lambda_1}{(2-1)(3-1)}\left(z'^{3-1} - (z'+t)^{3-1}\right) \tag{A17}$$

$$\vec{g} = -2\pi G\rho_{sm}\Lambda_1 t\hat{z} \tag{A18}$$

$$F_z^{(1)} = \vec{g}m_{tm} = -2\pi G\rho_{sm}\Lambda_1 t\hat{z}(\rho_{tm}\pi R^2 L) \tag{A19}$$

*Appendix B.2.* $n = 2$

$$dU = -G\rho_{sm}\Lambda_2 r_0\iiint\frac{dV_{sm}}{r^2} \tag{A20}$$

$$= -G\rho_{sm}\Lambda_2 r_0\iiint\frac{\rho d\rho d\theta dz}{\rho^2 + (z'-z)^2} \tag{A21}$$

Here the limits of integration for $\rho$ are $\rho \in [0,\rho_+]$. Integrating with respect to $\theta$ and making the following substitution $s = \rho^2 + (z'-z)^2$ gives

$$dU = -\pi G\rho_{sm}\Lambda_2 r_0\int_{(z'-z)^2}^{\rho_+^2+(z'-z)^2}\frac{ds}{s} \tag{A22}$$

$$U = -\pi G\rho_{sm}\Lambda_2 r_0\int_0^{-t}\ln\left(\frac{\rho_+^2 + (z'-z)^2}{(z'-z)^2}\right)dz \tag{A23}$$

$$\vec{g} = -\frac{dU}{dz}\hat{z} = \pi G\rho_{sm}\Lambda_2 r_0\frac{d}{dz}\int_0^{-t}\ln\left(\frac{\rho_+^2 + (z'-z)^2}{(z'-z)^2}\right)dz \tag{A24}$$

$$= \pi G\rho_{sm}\Lambda_2 r_0\left(\ln\left(\frac{\rho_+^2 + (z'+t)^2}{(z'+t)^2}\right) - \ln\left(\frac{\rho_+^2 + z'^2}{z'^2}\right)\right) \tag{A25}$$

$$= \pi G\rho_{sm}\Lambda_2 r_0\left(\ln\left(\frac{\rho_+^2 + (z'+t)^2}{\rho_+^2 + z'^2}\right) - \ln\left(\frac{(z'+t)^2}{z'^2}\right)\right) \tag{A26}$$

 doi:10.20944/preprints202402.1416.v1



Since we are considering the source mass as an infinite slab we take $\rho_+ \to +\infty$

$$\lim_{\rho_+ \to +\infty} \ln\left(\frac{\rho_+^2 + (z'+t)^2}{\rho_+^2 + z'^2}\right) = 0 \tag{A27}$$

$$\vec{g} = -\pi G \rho_{sm} \Lambda_2 r_0 \ln\left(\frac{(z'+t)^2}{z'^2}\right) \tag{A28}$$

$$F_z^{(2)} = \iiint \vec{g}(z') \rho_{tm} dx dy dz' \tag{A29}$$

$$F_z^{(2)} = -\pi G \rho_{sm} \rho_{tm} \Lambda_2 r_0 \iiint \ln\left(\frac{(z'+t)^2}{z'^2}\right) dx dy dz' \tag{A30}$$

The limits of integration over the cylindrical test mass are $x \in [-L/2, L/2]$, $y \in [0, \sqrt{R^2 - r^2}]$, and $r \in [-R, R]$ with $r = d + R - z'$ and $dr = -dz'$

$$F_z^{(2)} = -\pi G \rho_{sm} \rho_{tm} \Lambda_2 r_0 L \int_{-R}^{R} \int_0^{\sqrt{R^2-r^2}} \ln\left(\frac{(d+R+t-r)^2}{(d+R-r)^2}\right) dy(-dr) \tag{A31}$$

$$= -\pi G \rho_{sm} \rho_{tm} \Lambda_2 r_0 L \int_{-R}^{R} \sqrt{R^2 - r^2} \ln\left(\frac{(d+R+t-r)^2}{(d+R-r)^2}\right)(-dr) \tag{A32}$$

We could not find an analytical solution to the final integral, and it was solved numerically.

*Appendix B.3.* $n = 3$

$$dU = -G \rho_{sm} \Lambda_3 r_0^2 \iiint \frac{\rho d\rho d\theta dz}{(\rho^2 + (z'-z)^2)^{3/2}} \tag{A33}$$

Integrating $\theta$ and substituting $s^2 = (\rho^2 + (z'-z)^2)^{1/2}$

$$U = -2\pi G \rho_{sm} \Lambda_3 r_0^2 \int_0^{-t} \int_{z'-z}^{\infty} \frac{ds dz}{s^2} \tag{A34}$$

$$= -2\pi G \rho_{sm} \Lambda_3 r_0^2 \int_0^{-t} \frac{dz}{2(z'-z)} \tag{A35}$$

$$= \pi G \rho_{sm} \Lambda_3 r_0^2 \ln\left(\frac{z'+t}{z'}\right) \tag{A36}$$

$$\vec{g} = -\pi G \rho_{sm} \Lambda_3 r_0^2 \left(\frac{1}{z'+t} - \frac{1}{z'}\right) \tag{A37}$$

$$F_z^{(3)} = -\pi G \rho_{sm} \rho_{tm} \Lambda_3 r_0^2 \iiint \left(\frac{1}{z'+t} - \frac{1}{z'}\right) dx dy dz' \tag{A38}$$

 doi:10.20944/preprints202402.1416.v1



$$F_z^{(3)} = -\pi G\rho_{sm}\rho_{tm}\Lambda_3 r_0^2 L \int_{-R}^{R}\int_{0}^{\sqrt{R^2-r^2}} \left(\frac{-dydr}{d+R+t-r} + \frac{dydr}{d+R-r}\right) \tag{A39}$$

$$F_z^{(3)} = -\pi G\rho_{sm}\rho_{tm}\Lambda_3 r_0^2 L \int_{-R}^{R} \left(\frac{-\sqrt{R^2-r^2}}{d+R+t-r} + \frac{\sqrt{R^2-r^2}}{d+R-r}\right) dr \tag{A40}$$

$$F_z^{(3)} = -\pi G\rho_{sm}\rho_{tm}\Lambda_3 r_0^2 L \left(\frac{-\pi(d+R+t)^2}{2((d+R+t)^2-R^2)^{3/2}} + \frac{\pi(d+R)^2}{2((d+R)^2-R^2)^{3/2}}\right) \tag{A41}$$

*Appendix B.4.* $n = 4$

Starting with Eq. A15 for $n = 4$

$$U = \frac{-2\pi G\rho_{sm}\Lambda_4 r_0^3}{2}\left(\frac{1}{z'} - \frac{1}{z'+t}\right) \tag{A42}$$

$$\vec{g} = \pi G\rho_{sm}\Lambda_4 r_0^3(-z'^{-2} + (z'+t)^{-2}) \tag{A43}$$

$$F_z^{(4)} = -\pi G\rho_{sm}\Lambda_4 r_0^3 \iiint (z'^{-2} - (z'+t)^{-2})dxdydz' \tag{A44}$$

$$F_z^{(4)} = -\pi G\rho_{sm}\Lambda_4 r_0^3 L \int_{0}^{\sqrt{R^2-r^2}}\int_{-R}^{R} (z'^{-2} - (z'+t)^{-2})dy(-dr) \tag{A45}$$

$$F_z^{(4)} = -\pi G\rho_{sm}\rho_{tm}\Lambda_4 r_0^3 L \left(\frac{A_2\pi}{\sqrt{A_2^2-R^2}} - \frac{A_1\pi}{\sqrt{A_1^2-R^2}}\right) \tag{A46}$$

$A_2 = d+R+t$ and $A_1 = d+R$

*Appendix B.5.* $n = 5$

Starting with Eq. A15 for $n = 5$

$$U = \frac{-\pi G\rho_{sm}\Lambda_5 r_0^4}{3}\left(\frac{1}{z'^2} - \frac{1}{(z'+t)^2}\right) \tag{A47}$$

$$\vec{g} = \frac{-2\pi G\rho_{sm}\Lambda_5 r_0^4}{3}\left(\frac{1}{z'^3} - \frac{1}{(z'+t)^3}\right) \tag{A48}$$

$$F_z^{(5)} = \frac{-2\pi G\rho_{sm}\Lambda_5 r_0^4}{3}\iiint \left(\frac{1}{z'^3} - \frac{1}{(z'+t)^3}\right) dxdydz' \tag{A49}$$

$x \in [-L/2, L/2]$, $y \in [0, \sqrt{R^2-r^2}$, $r = d+R-z'$,
$dr = -dz'$

$$F_z^{(5)} = \frac{-\pi G\rho_{sm}\Lambda_5 r_0^4 L}{3}\left(\frac{A_1^2}{(A_1^2-R^2)^{3/2}} - \frac{A_2^2}{(A_2^2-R^2)^{3/2}}\right) \tag{A50}$$

$A_2 = d+R+t$ and $A_1 = d+R$

## References


1. Langacker, P. *The standard model and beyond*; Taylor & Francis, 2017.
2. Kiefer, C. *Why quantum gravity?*; Springer, 2007.
3. Rovelli, C. *Quantum gravity*; Cambridge university press, 2004.
4. Weinberg, S. A new light boson? *Physical Review Letters* **1978**, *40*, 223.
5. Klimchitskaya, G.L.; Mostepanenko, V.M. Dark Matter Axions, Non-Newtonian Gravity and Constraints on Them from Recent Measurements of the Casimir Force in the Micrometer Separation Range. *Universe* **2021**, *7*, 343.
6. Banks, H.; McCullough, M. Charting the fifth force landscape. *Physical Review D* **2021**, *103*, 075018.
7. Adelberger, E.; Heckel, B.R.; Hoedl, S.; Hoyle, C.; Kapner, D.; Upadhye, A. Particle-physics implications of a recent test of the gravitational inverse-square law. *Physical Review Letters* **2007**, *98*, 131104.
8. Klimchitskaya, G.L. Constraints on Theoretical Predictions beyond the Standard Model from the Casimir Effect and Some Other Tabletop Physics. *Universe* **2021**, *7*. https://doi.org/10.3390/universe7030047.
9. Adelberger, E.; Heckel, B.; Nelson, A. TESTS OF THE GRAVITATIONAL INVERSE-SQUARE LAW. *Annual Review of Nuclear and Particle Science* **2003**, *53*, 77–121, [https://doi.org/10.1146/annurev.nucl.53.041002.110503]. https://doi.org/10.1146/annurev.nucl.53.041002.110503.
10. Tan, W.H.; Du, A.B.; Dong, W.C.; Yang, S.Q.; Shao, C.G.; Guan, S.G.; Wang, Q.L.; Zhan, B.F.; Luo, P.S.; Tu, L.C.; et al. Improvement for testing the gravitational inverse-square law at the submillimeter range. *Physical Review Letters* **2020**, *124*, 051301.
11. Chen, Y.J.; Tham, W.K.; Krause, D.E.; López, D.; Fischbach, E.; Decca, R.S. Stronger Limits on Hypothetical Yukawa Interactions in the 30–8000 nm Range. *Phys. Rev. Lett.* **2016**, *116*, 221102. https://doi.org/10.1103/PhysRevLett.116.221102.
12. Timberlake, C.; Vinante, A.; Shankar, F.; Lapi, A.; Ulbricht, H. Probing modified gravity with magnetically levitated resonators. *Physical Review D* **2021**, *104*, L101101.
13. Westphal, T.; Hepach, H.; Pfaff, J.; Aspelmeyer, M. Measurement of gravitational coupling between millimetre-sized masses. *Nature* **2021**, *591*, 225–228.
14. Sedmik, R.I.P.; Pitschmann, M. Next Generation Design and Prospects for Cannex. *Universe* **2021**, *7*. https://doi.org/10.3390/universe7070234.
15. Barker, P.F.; Bose, S.; Marshman, R.J.; Mazumdar, A. Entanglement based tomography to probe new macroscopic forces. *Physical Review D* **2022**, *106*, L041901.
16. Shi, H.; Zhuang, Q. Ultimate precision limit of noise sensing and dark matter search. *npj Quantum Information* **2023**, *9*, 27.
17. Moore, D.C.; Geraci, A.A. Searching for new physics using optically levitated sensors. *Quantum Science and Technology* **2021**, *6*, 014008. https://doi.org/10.1088/2058-9565/abcf8a.
18. Kawasaki, A. Measurement of the Newtonian constant of gravitation G by precision displacement sensors. *Classical and Quantum Gravity* **2020**, *37*, 075002. https://doi.org/10.1088/1361-6382/ab6f80.
19. Tino, G.M. Testing gravity with cold atom interferometry: results and prospects. *Quantum Science and Technology* **2021**, *6*, 024014. https://doi.org/10.1088/2058-9565/abd83e.
20. Decca, R.; Lopez, D.; Chan, H.; Fischbach, E.; Krause, D.; Jamell, C. Constraining new forces in the Casimir regime using the isoelectronic technique. *Physical Review Letters* **2005**, *94*, 240401.
21. Virtanen, P.; Gommers, R.; Oliphant, T.E.; Haberland, M.; Reddy, T.; Cournapeau, D.; Burovski, E.; Peterson, P.; Weckesser, W.; Bright, J.; et al. SciPy 1.0: Fundamental Algorithms for Scientific Computing in Python. *Nature Methods* **2020**, *17*, 261–272. https://doi.org/10.1038/s41592-019-0686-2.
22. Bsaibes, T.; Pires, L.; Czaplewski, D.; López, D.; Decca, R.S. Toward a better system for short range precision force measurements. *Modern Physics Letters A* **2020**, *35*, 2040002, [https://doi.org/10.1142/S0217732320400027]. https://doi.org/10.1142/S0217732320400027.